A rapidly magnetically assembled stem cell microtissue with "hamburger" architecture and enhanced vascularization capacity

Yuezhi Lu [a,1], Chun-Hua Yu [a,1], Guangzheng Yang [a], Ningjia Sun [a], Fei Jiang [a], Mingliang Zhou [a], Xiaolin Wu [a], Jiaxin Luo [a], Cui Huang [b], Wenjie Zhang [a,**], Xinquan Jiang [a,*]

[a] Department of Prosthodontics, Shanghai Engineering Research Center of Advanced Dental Technology and Materials, Shanghai Key Laboratory of Stomatology & Shanghai Research Institute of Stomatology, National Clinical Research Center for Oral Diseases, Shanghai Ninth People's Hospital, College of Stomatology, Shanghai Jiao Tong University School of Medicine, Shanghai, 200011, China

[b] The State Key Laboratory Breeding Base of Basic Science of Stomatology and Key Laboratory for Oral Biomedical Ministry of Education, School & Hospital of Stomatology, Wuhan University, Wuhan, Hubei, 430079, China

A B S T R A C T

With the development of magnetic manipulation technology based on magnetic nanoparticles (MNPs), scaffold-free microtissues can be constructed utilizing the magnetic attraction of MNP-labeled cells. The rapid *in vitro* construction and *in vivo* vascularization of microtissues with complex hierarchical architectures are of great importance to the viability and function of stem cell microtissues. Endothelial cells are indispensable for the formation of blood vessels and can be used in the prevascularization of engineered tissue constructs. Herein, safe and rapid magnetic labeling of cells was achieved by incubation with MNPs for 1 h, and ultrathick scaffold-free microtissues with different sophisticated architectures were rapidly assembled, layer by layer, in 5 min intervals. The *in vivo* transplantation results showed that in a stem cell microtissue with trisection architecture, the two separated human umbilical vein endothelial cell (HUVEC) layers would spontaneously extend to the stem cell layers and connect with each other to form a spatial network of functional blood vessels, which anastomosed with the host vasculature. The "hamburger" architecture of stem cell microtissues with separated HUVEC layers could promote vascularization and stem cell survival. This study will contribute to the construction and application of structural and functional tissues or organs in the future.

1. Introduction

Stem cell-based therapies have shown great potential in the treatment of various diseases and tissue repair [1–3]. A major obstacle to stem cell-based tissue regeneration is that the transplanted stem cells are prone to death prior to differentiation into the desired cell types, due to lack of oxygen and nutrient supplies [4]. The rapid formation of vascular network and its anastomosis with the host vasculature are critical to the early survival of stem cells by providing oxygen and nutrients and removing metabolic wastes [5]. The lack of vascularization also limits the size of transplanted microtissues or organoids, since the growth of tissues *in vivo* is supported by a complex network of vasculature [6,7].

The assembly of living cells without biomaterials has opened up a new avenue to construct customized tissues or organoids with complex architectures [8,9]. The classic method of cell sheet preparation is based on a temperature-responsive culture surface. The cells are inoculated on the temperature-responsive culture surface and cultured at 37 °C, and the monolayer cell sheet is harvested when the temperature is below 32 °C [10,11]. Although the approach is easy to follow, it is difficult to obtain a thick cell sheet/microtissue with a complex architecture directly and rapidly. *In vitro* assembled microtissues preserve the extracellular matrix (ECM) and cell-cell interactions, as well as 3D tissue structures. Thus, they more closely resemble *in vivo* tissues, and are more conducive to the therapeutic efficacy of stem cell-based therapies after *in vivo* transplantation [12–15].

Magnetic nanoparticles (MNPs) are widely used in biomedicine

because of their excellent biocompatibility and superparamagnetic properties, and have been approved for clinical use by the FDA [16–18]. Remote magnetic manipulation and image tracking of microtissues can be performed because MNPs can be manipulated by remote magnetic fields and detected [19,20]. Magnetic cell sheet preparation was first proposed by Ito et al. that multilayered keratinocyte sheets were assembled using MNPs and magnetic force [21]. In recent years, with the development of magnetic manipulation technology, it has been realized to assemble cell sheets/microtissues with thicker dimensions, more complex shapes, and containing different cell types [22–25]. The cells in the ultrathick microtissues are prone to necrosis after long time culture *in vitro* and transplantation *in vivo* due to insufficient nutrient and oxygen supply and inefficient exchange of metabolic wastes [4,26,27]. It is of great importance to optimize the magnetic labeling and assembly time for rapid construction of microtissues with complex 3D architectures. Rapid vascularization *in vivo* is essential for cell survival when the microtissue diameter exceeds 200 µm [28].

Dental pulp stem cells (DPSCs) have strong capacities for self-renewal, proliferation, and differentiation to regenerate dentin and dental pulp tissue [29,30]. Because the root canal system of the tooth is narrow and curved, and the narrow apical foramen is the main channel of blood vessels, the application of DPSC microtissues for dental pulp regeneration has a strong demand for vascularization [31]. Endothelial cells are indispensable for the formation of blood vessels and can be used in the prevascularization of engineered tissue constructs [32–34]. The co-culture of stem cells with endothelial cells has been shown to be a very effective strategy to promote vascularization and tissue regeneration [35–38]. However, few studies have focused on the spatial ordered combination of stem cells and endothelial cells, and it is unknown whether the assembly of stem cells and endothelial cells into geometric architectures is beneficial to the survival of stem cell microtissues.

In this study, we optimized the minimum time required to magnetically label DPSCs and human umbilical vein endothelial cells (HUVECs) with MNPs. Scaffold-free 3D microtissues with different sophisticated architectures could thus be rapidly assembled layer by layer, using MNP-labeled DPSCs and HUVECs, and the dimensions were measured based on the 3D reconstruction of micro-CT. Similar to the architecture of a hamburger, a common food containing multiple layers of breads and meats, DPSC-trisection microtissue was assembled by adding DPSCs and HUVECs layer by layer. *In vivo* transplantation of the assembled microtissues demonstrated that the HUVEC layers spontaneously extended to the DPSC layers. In the "hamburger" microtissues with trisection DPSC layers, the two separated HUVEC layers would connect to each other to form a spatial network of functional blood vessels that anastomosed with the host vasculature, thereby promoting the vascularization and survival of DPSC microtissues.

2. Materials and methods

2.1. Cell culture

DPSCs were isolated from extracted orthodontic teeth or third molars of healthy donors, using the method described in our previous study, with the approval of the Ethics Committee of Shanghai Ninth People's Hospital [39]. Briefly, the dental pulp tissues were isolated, minced into 1–2 mm^3 pieces, and then digested with 4 mg mL^{-1} dispase and 3 mg mL^{-1} collagenase type I in PBS for 1 h at 37 °C, with vigorous shaking. After centrifugation, the supernatant was removed and the remaining cells were cultured in alpha-modified Eagle's medium (Gibco, USA) containing 1% penicillin-streptomycin (Sigma, USA) and 10% fetal bovine serum (Gibco, USA). HUVECs were purchased from ScienCell Research Laboratories (Carlsbad, CA, USA). Cells of passage 3–7 were used for the subsequent experiments.

2.2. Magnetic labeling of cells

MNPs with an average diameter of 50 nm were purchased from Micxy Reagent Co., Ltd. (Chengdu, China). After disinfection in 75% alcohol and washing with PBS, the dispersion of MNPs was diluted to 100 µg mL^{-1} using serum-free high glucose DMEM. Cells were incubated with 100 µg mL^{-1} MNP medium from 10 min to 8 h to screen the optimal time for magnetic labeling, and the MNPs not swallowed by the cells in the medium were washed away. Cells were stained using a Prussian Blue Iron Stain Kit (Polysciences, USA), according to the manufacturer's instructions. To confirm the safety of magnetic labeling, cells were incubated with 100 µg mL^{-1} MNPs from 30 min to 8 h, and evaluated using an Annexin V-FITC/PI detection kit (BD Biosciences, USA), following the manufacturer's instructions, as previously described [40]. Cell apoptosis and necrosis were measured using flow cytometry, and the data were analyzed using FlowJo V10.0 (Treestar, Ashland, OR, USA). The percentage of apoptotic and necrotic cells was calculated.

2.3. Magnetic attraction of cells

Approximately one million DPSCs and one million HUVECs were incubated with 100 µg mL^{-1} MNP medium from 30 min to 2 h, and then attracted using the Neodymium-ironboron permanent magnets with a diameter of 3 mm, to form a layer of cells. Cells that were not attracted by the magnets were washed away immediately using PBS. After 4 h, cells were fixed with 4% paraformaldehyde and stained using DAPI (Beyotime, Shanghai, China). The magnets were removed and images of the cell sheets were obtained using a confocal laser scanning microscope (Leica, Germany). The number of DPSCs and HUVECs was calculated using ImageJ software [41].

2.4. Assembly of 3D microtissues

To track cells *in vitro*, DPSCs were labeled with 3,3-dioctadecyloxacarbocyanine perchlorate (DiO), and HUVECs were labeled with 1,1′-Dioctadecyl-3,3,3′,3′-tetramethylindocarbocyanine perchlorate (DiI). DPSCs and HUVECs were incubated with 100 µg mL^{-1} MNPs for 1 h to accomplish magnetic labeling. Neodymium-ironboron permanent magnets with a diameter of 3 mm were used under the bottom of culture dishes to attract cells. Approximately one million cells were added each time to the culture dish to form one layer of the microtissue via magnetic attraction. Approximately 5 min later, the bottom layer was stable enough to add the next one million cells to form the next layer of the microtissue. A multilayered microtissue with a sophisticated architecture was rapidly assembled layer by layer by repeatedly adding MNP-labeled cells. After 24 h of *in vitro* culture, neodymium-ironboron permanent magnets were removed and microtissues were harvested from the culture dishes for subsequent studies.

2.5. Micro-CT

After 24 h of *in vitro* culture, the microtissues were fixed with 4% paraformaldehyde and then scanned using micro-CT (Scanco Medical, Switzerland), and each scanning layer had a thickness of 10 µm. 3D reconstruction and 2D images from different observation directions of the microtissues were carried out using the micro-CT system software. The diameter and height of the microtissues were measured using the micro-CT system software.

2.6. In vitro cell staining

After 24 h of *in vitro* culture, the microtissues were fixed with 4% paraformaldehyde, embedded in optimum cutting temperature (OCT) compound (Thermo Fisher, USA) and frozen. Serial sections with a slice thickness of 4 µm were prepared for immunofluorescence staining. Nuclei were stained with DAPI (Beyotime, Shanghai, China). The

architectures of DiO + DPSC layers and DiI + HUVEC layers in micro-tissues were observed using a fluorescence microscope.

2.7. In vivo transplantation

All animals used in this study were provided by the Ninth People's Hospital Animal Center (Shanghai, China). All experimental protocols performed in this study were approved by the Animal Care and Experiment Committee of the Ninth People's Hospital. To track cells *in vivo*, DPSCs were transfected with a green fluorescent protein (GFP) lentivirus and HUVECs were transfected with a red fluorescent protein (RFP) lentivirus. Five million DPSCs were divided into five equal parts, and then added layer by layer to assemble DPSC microtissues. To assemble DPSC-bisection microtissues, five million DPSCs divided into four equal parts and one million HUVECs as another one part, were added layer by layer to form the bottom two layers of DPSCs, the middle layer of HUVECs, and the top two layers of DPSCs. To assemble DPSC-trisection microtissues, five million DPSCs divided into three equal parts and one million HUVECs divided into two equal parts, were added layer by layer. After 24 h of *in vitro* culture, the microtissues with a diameter of 3.5 mm and a height of 400 μm were transplanted into 8-week-old male nude (BALB/c-nu) mice. After anesthesia, four subcutaneous pockets were formed on the dorsal side of each nude mouse for microtissue transplantation.

2.8. Microfil perfusion

Nude mice were perfused with microfil (Flow Tech, Carver, MA, USA), as previously described [42]. After subcutaneous transplantation for 3 days, the nude mice were anesthetized. The abdominal aorta was exposed and penetrated with an angio-catheter. Each nude mouse was perfused with a total of 10 mL of microfil. The nude mice were placed at 4 °C for 1 h for microfil coagulation. The samples were extracted, frozen into sections, and fixed for subsequent HE and immunofluorescent staining.

2.9. Immunohistochemical analysis

Nude mice were sacrificed 3 and 7 days after subcutaneous transplantation. The samples were fixed with formalin, embedded in OCT compound, and frozen. Serial sections with a slice thickness of 4 μm were prepared for HE staining and CD31 immunofluorescence staining. Primary antibodies against CD31 (R&D Systems, USA) and rabbit anti-goat IgG secondary antibodies (Abcam, USA) were used, followed by counterstaining of cellular nuclei with DAPI. Images were obtained using a confocal laser scanning microscope (Leica, Germany). The positive area was captured and calculated using ImageJ software for statistical analysis [41]. After observation under a confocal laser scanning microscope, the sections were restained with HE.

2.10. Statistical analysis

Data were presented as mean ± standard deviation. Statistical analysis was performed using the GraphPad Prism 8.0 software. Comparisons between groups were analyzed using one-way analysis of variance, followed by Tukey's multiple comparisons test. A $p < 0.05$ or $p < 0.01$ indicated a statistically significant difference.

3. Results and discussion

3.1. Safe and rapid magnetic labeling of DPSCs and HUVECs

A safe and rapid magnetic labeling of DPSCs and HUVECs is of great benefit to shorten the preparation time before the magnetic assembly of microtissues. We used MNPs with a concentration of 100 μg mL^{-1}, which was optimized in our previous study [23]. The Prussian blue

staining results indicated that the intracellular MNP content increased in a time-dependent manner (Fig. 1a). Previous studies have shown that the addition of magnetic materials, such as MNPs, does not affect the long-term behavior of cells [43,44]. To verify the short-term effects of the accumulated MNPs in cells as the magnetic labeling time increased, DPSCs and HUVECs were incubated with 100 μg mL^{-1} MNPs up to 8 h, and then cell apoptosis and necrosis were evaluated using flow cytometry. According to the Annexin V fluorescein isothiocyanate and propidium iodide (Annexin V FITC/PI) analysis using flow cytometry (Fig. 1b), there were no significant differences in the percentage of both early apoptosis (Fig. 1c), and late apoptosis and necrosis (Fig. 1d) among DPSCs magnetically labeled for different times (0, 0.5, 1, 2, 4, and 8 h). After 2 d of subsequent culture, the Annexin V FITC/PI analysis showed no significant differences in the percentage of both early apoptosis (Fig. 1e), and late apoptosis and necrosis (Fig. 1f) among DPSCs magnetically labeled for different times (0, 0.5, 1, 2, 4, and 8 h). Similar trends were also found in the magnetic labeling of HUVECs. The Annexin V FITC/PI analysis of HUVECs (Fig. 1g) showed no significant differences in the percentage of both early apoptosis (Fig. 1h), and late apoptosis and necrosis (Fig. 1i) among HUVECs magnetically labeled for different times (0, 0.5, 1, 2, 4, and 8 h). After 2 d of subsequent culture, the Annexin V FITC/PI analysis showed no significant differences in the percentage of both early apoptosis (Fig. 1j), and late apoptosis and necrosis (Fig. 1k) among HUVECs magnetically labeled for different times (0, 0.5, 1, 2, 4, and 8 h).

To optimize the magnetic labeling time, DPSCs and HUVECs were incubated with MNPs for a period of time to determine the shortest incubation time necessary for remote magnetic manipulation of cells. To track cells *in vitro*, DPSCs were labeled with DiO, and HUVECs were labeled with DiI (Fig. S1a). Flow cytometry results showed that 99.7% of DPSCs (Fig. S1b) and 99.1% of HUVECs (Fig. S1c) were validly labeled. After incubation with MNPs for 30 min to 2 h, MNP-labeled cells were added to the culture dishes and were immediately attracted by magnets (Fig. 2a and b). There were no significant differences in the DPSC number attracted by magnets among the different magnetic labeling times (30 min, 1 h, and 2 h), although a slight increase was observed for 1 h, compared to 30 min of labeling time (Fig. 2c). Regarding the HUVEC number attracted by magnets, there was a significant difference between the 30 min and 1 h labeling times, while no significant difference was found between 1 h and 2 h (Fig. 2d). These results indicated that when DPSCs and HUVECs were magnetically labeled with 100 μg mL^{-1} MNPs, an incubation time of 1 h was sufficient for the magnetic manipulation of cells.

Based on the safe and effective MNP concentration discovered in our previous study [23], we further confirmed that cells incubated with 100 μg mL^{-1} MNPs for a long time had no significant effect on apoptosis and necrosis. As with many previous studies, the safety of labeling cells with MNPs was assured [16–18,23,24]. Nevertheless, for the magnetic assembly of microtissues, on the premise of ensuring MNP-labeled cells that could be manipulated by the remote magnetic field, a shorter MNP incubation time would make the construction of microtissues more practical and benefit the assembly of complex architectures. Compared with the previous method, the magnetic labeling time was shortened to 1 h in the study [23,24].

3.2. Assembly of 3D microtissues with sophisticated architectures

The remote magnetic assembly of 3D microtissues is one of the advantages of using MNP-labeled cells. In this study, DPSCs and HUVECs were incubated with 100 μg mL^{-1} MNPs for 1 h to accomplish rapid magnetic labeling. Then, the added MNP-labeled cells were immediately dragged down to the bottom of the cell culture dish using magnets to assemble the first layer of the microtissue. After 5 min, the second layer of the microtissue was assembled by addition of MNP-labeled cells. A multilayered microtissue with a sophisticated architecture was assembled layer by layer by repeatedly adding MNP-labeled cells (Fig. 3a).
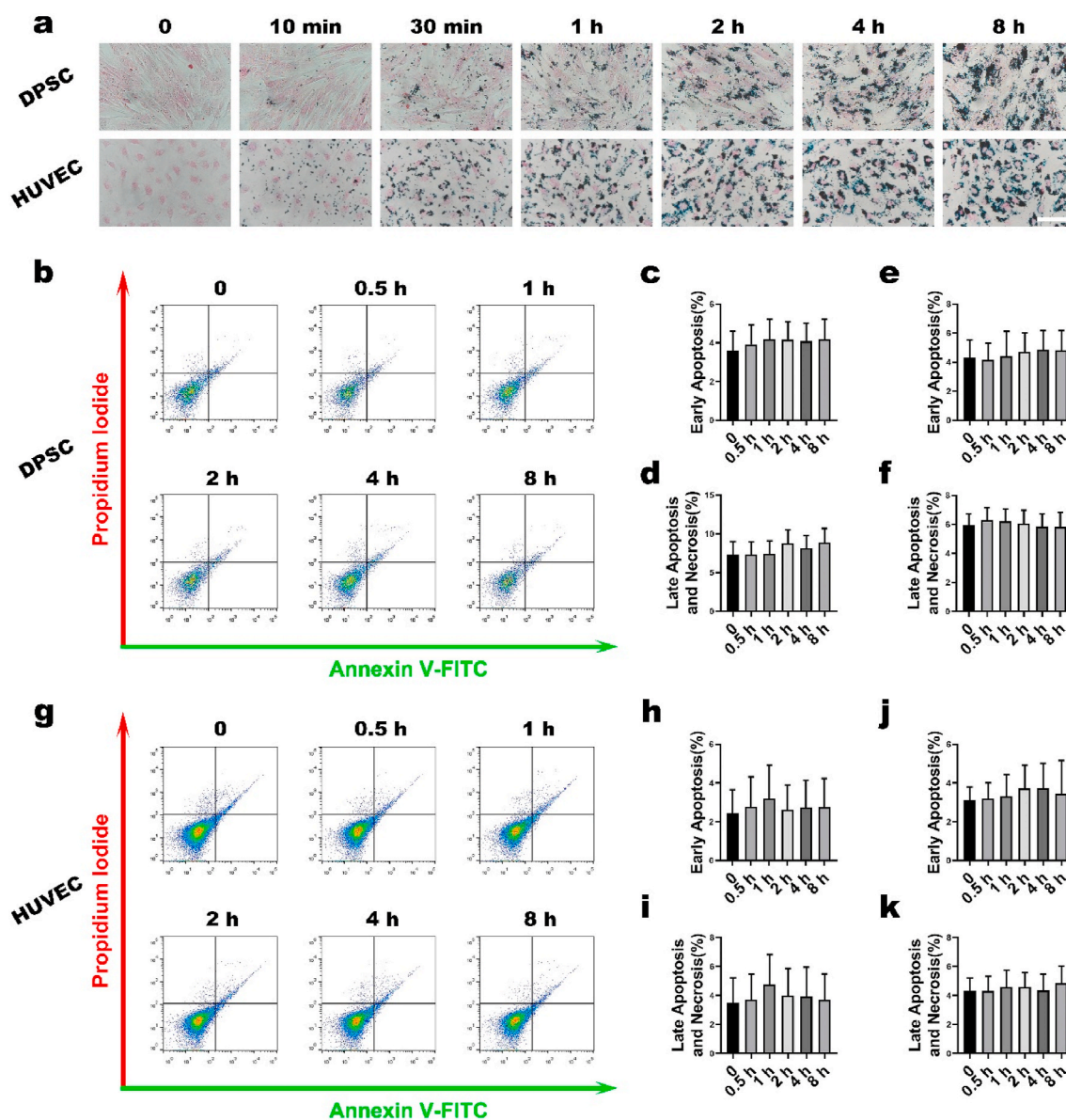
Fig. 1. Safe magnetic labeling of DPSCs and HUVECs. a) DPSCs and HUVECs were incubated with 100 μg mL^{-1} MNPs for times ranging from 10 min to 8 h. Prussian-blue staining was used to visualize the distribution of MNPs (scale bar: 100 μm). b) DPSCs were incubated with 100 μg mL^{-1} MNPs from 30 min to 8 h, and the apoptosis and necrosis were measured immediately after MNP incubation using flow cytometry. c) The percentage of early apoptosis of DPSCs immediately after MNP incubation was calculated. d) The percentage of late apoptosis and necrosis of DPSCs immediately after MNP incubation was calculated. e) The percentage of early apoptosis of DPSCs 2 d after MNP incubation was calculated. f) The percentage of late apoptosis and necrosis of DPSCs 2 d after MNP incubation was calculated. g) HUVECs were incubated with 100 μg mL^{-1} MNPs from 30 min to 8 h, and the apoptosis and necrosis were measured immediately after MNP incubation using flow cytometry. h) The percentage of early apoptosis of HUVECs immediately after MNP incubation was calculated. i) The percentage of late apoptosis and necrosis of HUVECs immediately after MNP incubation was calculated. j) The percentage of early apoptosis of HUVECs 2 d after MNP incubation was calculated. k) The percentage of late apoptosis and necrosis of HUVECs 2 d after MNP incubation was calculated.

The dimensions of the assembled microtissues could be measured based on the 3D reconstruction of the micro-CT, owing to the properties of MNPs [45]. One million DPSCs were added to the culture dish as one layer. DPSCs were preferentially attracted to the edge of the magnet to form the first layer with a ring structure. As more cells were added, the microtissue gradually grew larger and thicker into a solid pie structure (Fig. 3b). The diameter and height of the microtissues increased quickly at the start, and there were significant differences among one, three, and five layers of the microtissues. However, after the microtissues exceeded five layers, the diameter and height increased slowly, and there was no significant difference between the microtissues with five or seven layers (Fig. 3d and e).

Multilayered microtissues with sophisticated 3D architectures can be assembled based on magnetic manipulation technology. Microtissues with different layers and thicknesses, such as two (DH), three (DHD), five (DHDHD), and seven (DHDHDHD) layers, were assembled by orderly adding DiO positive (DiO+) DPSCs and DiI positive (DiI+) HUVECs, layer by layer, with 5 min intervals between each layer (Fig. 4a). Microtissues with the same layers but different patterns could also be assembled. For example, five-layered microtissues could be assembled by adding five layers of DiO + DPSCs (DDDDD/DPSC), or by adding two layers of DiO + DPSCs, one layer of DiI + HUVECs, and two layers of DiO + DPSCs (DDHDD/DPSC-bisection), or by adding DiO + DPSCs and DiI + HUVECs, layer by layer (DHDHD/DPSC-trisection), for a total of five times (Fig. 4b).

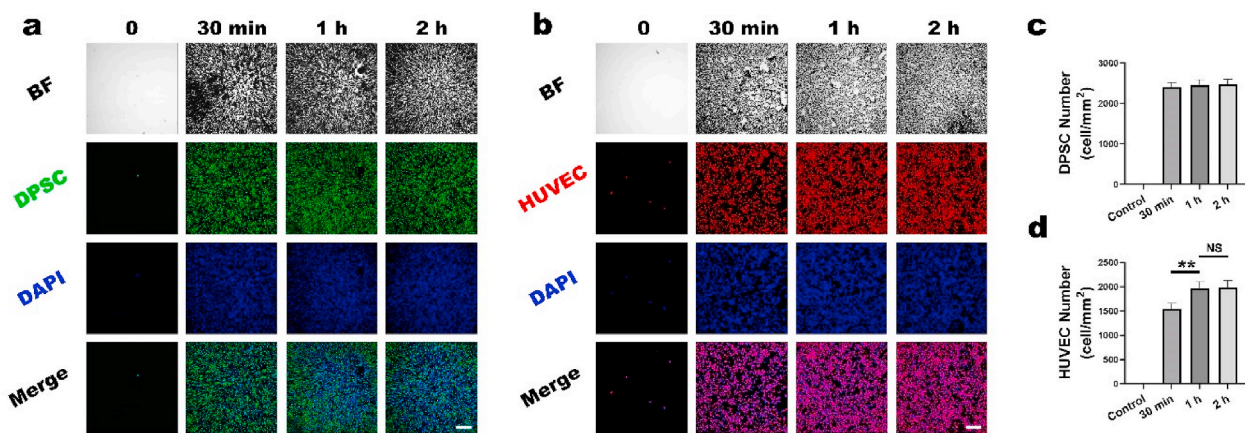Traditional monolayer cell culture cannot be used to construct 3D

Fig. 2. Rapid magnetic labeling of DPSCs and HUVECs. a) DPSCs were incubated with 100 μg mL^{-1} MNPs for times ranging from 30 min to 2 h, and then added to the culture dishes and attracted by magnets. Cells that were not attracted by magnets were washed away immediately. Four hours later, cell deposition was visualized using a confocal laser scanning microscope (scale bar: 200 μm). b) HUVECs were incubated with 100 μg mL^{-1} MNPs from 30 min to 2 h, and then added to the culture dishes and attracted by magnets. Cells that were not attracted by magnets were washed away immediately. Four hours later, cell deposition was visualized using a confocal laser scanning microscope (scale bar: 200 μm). c) The number of DPSC per mm^2 was calculated using ImageJ software. d) The number of HUVEC per mm^2 was calculated using ImageJ software (** represents $p < 0.01$).
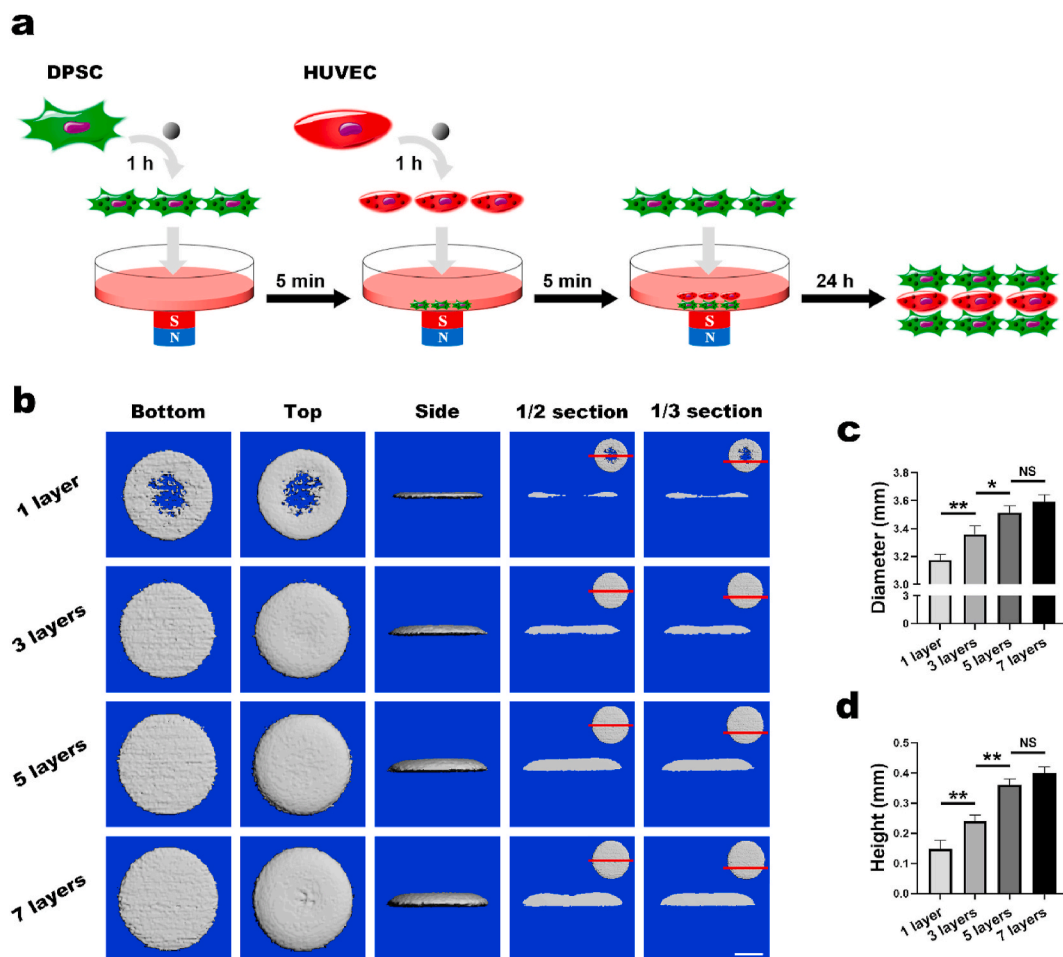

Fig. 3. Assembly strategies and 3D dimensions of microtissues. a) The assembly schematic diagram of multilayered microtissues. b) The assembled microtissues were scanned using a micro-CT and the 3D images were obtained via 3D reconstruction (scale bar: 1 mm). c, d) The diameter (c) and height (d) of microtissues were measured using the micro-CT system software (* represents $p < 0.05$, ** represents $p < 0.01$).

tissues in the absence of supporting biomaterials due to contact inhibition [46–50]. Bioprinting technology can construct 3D tissues layer by layer using cell-laden bioinks, but it usually relies on biomaterials such as hydrogels and fibers as carriers for living cells, as well as expensive specialized bioprinting equipment [9,51]. Traditional cell sheet technology can construct monolayer cell sheets that preserve ECM and
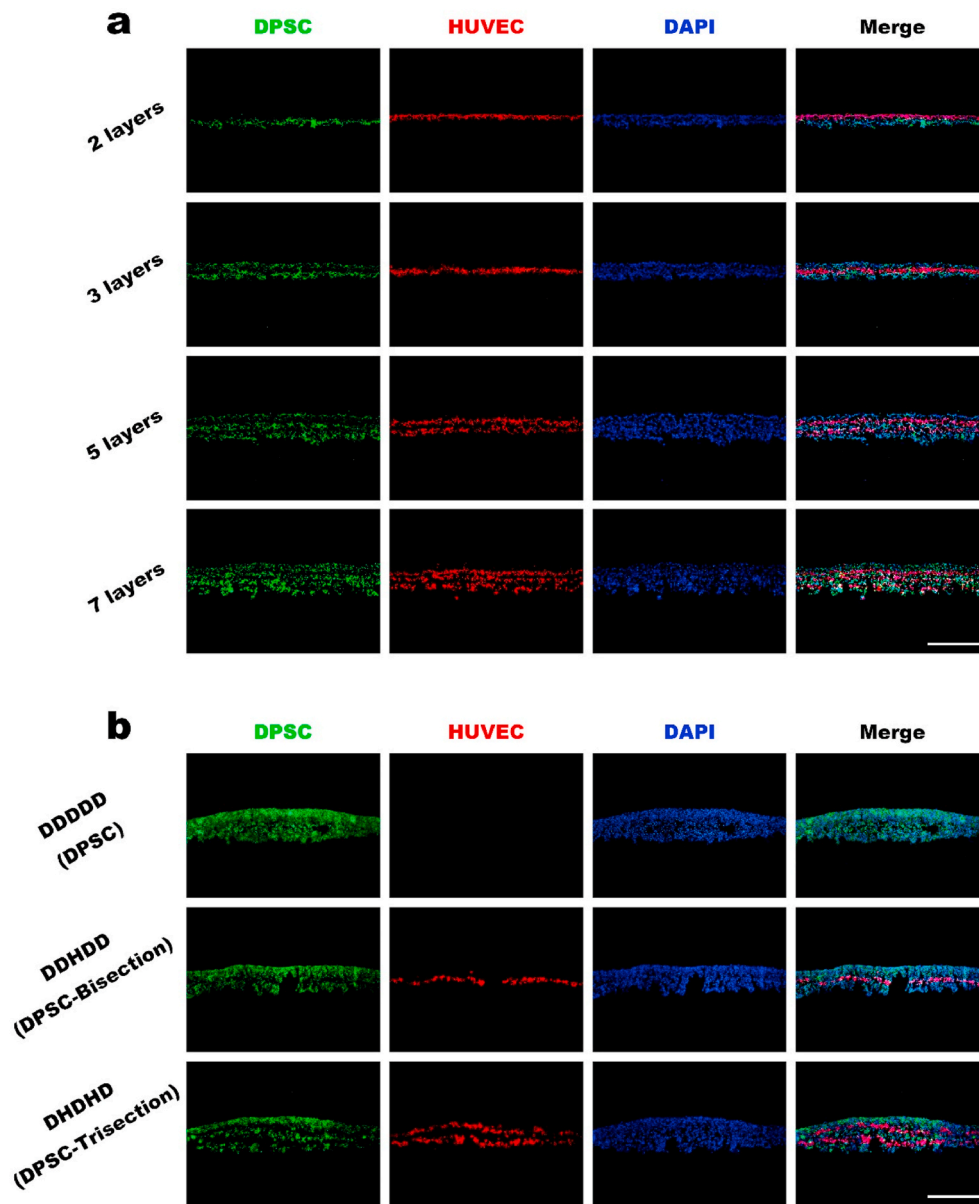
Fig. 4. Assembly of microtissues with sophisticated architectures. a) Assembly of microtissues with different layers and thickness (scale bar: 500 μm). b) Assembly of microtissues with the same layers, but with different patterns (scale bar: 500 μm).

cell-cell interactions without biomaterials [26]. However, it usually takes more than one week to construct a monolayer cell sheet with a limited thickness. Based on the magnetic assembly method of thick cell sheets in our previous study [23], we successfully assembled scaffold-free microtissues with different sophisticated architectures by adding MNP-labeled cells layer by layer in a very short time. It took about 30 min to assemble 7 layers of microtissue. Cells of each layer were immediately attracted by a magnet, with 5 min intervals between layers. Our simple and practical method of microtissue construction is similar to bioprinting to some extent, but it does not rely on biomaterials or specialized equipment.

3.3. Rapid vascularization and increased cell survival of in vivo transplanted microtissues

To track cells *in vivo*, DPSCs and HUVECs were transfected with GFP and RFP lentiviruses, respectively (Fig. S1a). Flow cytometry results showed that the positive GFP (GFP+) ratio of DPSCs was 95.2%

(Fig. S1d) and the positive RFP (RFP+) ratio of HUVECs was 94.1% (Fig. S1e). In order to clarify the role of the multisection architecture in vascularization and stem cell survival of the microtissues, DPSC microtissues were assembled using five million GFP + DPSCs. DPSC-bisection microtissues were assembled using five million GFP + DPSCs separated into two sections, with one million RFP + HUVECs in the middle. DPSC-trisection microtissues were assembled using five million GFP + DPSCs separated into three sections, and one million RFP + HUVECs separated into two sections among the DPSC sections. After 24 h of *in vitro* culture, the assembled microtissues gradually became solid and could be transplanted *in vivo* (Fig. 3a).

Hematoxylin-eosin (HE) staining showed that, after 3 days of subcutaneous transplantation into nude mice, the microtissues of different groups were all well integrated with the host tissues (Fig. 5a). Compared with the DPSC microtissue, although the positive GFP area in the DPSC-bisection microtissue was slightly higher, the difference was not statistically significant. The positive GFP area in the DPSC-trisection microtissue was higher than that in the DPSC microtissue and the DPSC-
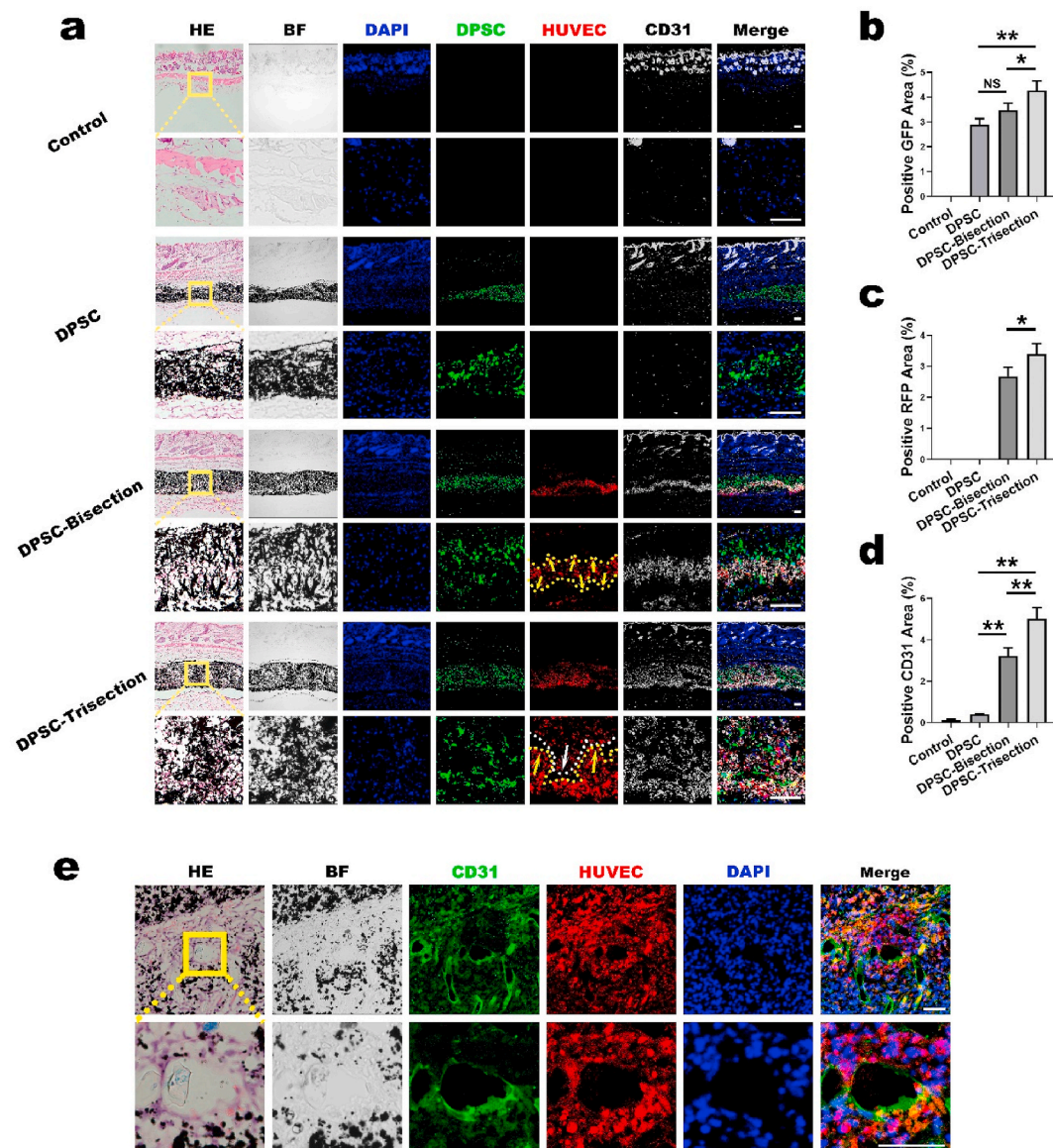
Fig. 5. *In vivo* transplantation of microtissues for 3 days. a) HE staining and CD31 immunofluorescent staining of the Control group, DPSC microtissue group, DPSC-bisection microtissue group, and DPSC-trisection microtissue group (scale bar: 100 μm). The dotted lines in the DPSC-bisection microtissue group show the boundaries of the HUVEC layer. The arrows in the DPSC-bisection microtissue group indicate that the HUVEC layer begins to extend to the DPSC layer. The yellow dotted line in the DPSC-trisection microtissue group shows the upper boundary of the lower HUVEC layer. The white dotted line in the DPSC-trisection microtissue group shows the lower boundary of the upper HUVEC layer. The yellow arrows in the DPSC-trisection microtissue group indicate that the lower HUVEC layer begins to extend and connect to the upper HUVEC layer. The white arrow in the DPSC-trisection microtissue group indicates that the upper HUVEC layer begins to extend and connect to the lower HUVEC layer. b) Positive GFP area in four groups. c) Positive RFP area in four groups. d) Positive CD31 area in four groups. e) HE staining and CD31 immunofluorescent staining of the DPSC-trisection microtissue group after microfil perfusion (scale bar: 50 μm).

bisection microtissue, which indicated improved stem cell survival (Fig. 5b). The integrated RFP + HUVEC layer in the DPSC-bisection microtissue began to extend to the adjacent GFP + DPSC layers, while the two separated RFP + HUVEC layers in the DPSC-trisection microtissue not only began to extend to the adjacent GFP + DPSC layers, but also began to connect with each other to form a vascular network (Fig. 5a). The positive RFP area in the DPSC-trisection microtissue was higher than that in the DPSC-bisection microtissue (Fig. 5c). CD31 immunofluorescent staining was performed to better visualize the capillary-like structures. The positive CD31 area in the DPSC-bisection microtissue was higher than that in the DPSC microtissue, while that in the DPSC-trisection microtissue was higher than that in the DPSC-bisection microtissue (Fig. 5d). These results indicated that the DPSC-trisection microtissue had the best vascularization and highest stem cell survival (Fig. 5a).

In order to verify the function of the capillary-like structures formed by HUVECs, microfil perfusion was performed 3 days after subcutaneous implantation into nude mice. HE staining showed that a blue microfil agent was observed in the capillary-like structure. CD31 immunofluorescent staining and RFP + HUVECs showed that the capillary-like structure was formed by HUVECs (Fig. 5e). These results indicated that as early as 3 days post-transplantation, the capillary-like structures formed by HUVECs were well anastomosed with the host vasculature and performed a vascular function in the microtissues.

Similar trends were also observed after 7 days of subcutaneous transplantation into nude mice. The RFP + HUVEC layer extended more obviously to the adjacent DPSC layers in the DPSC-bisection microtissue than at 3 days, and the separated two RFP + HUVEC layers in the DPSC-trisection microtissue extended to each other and connected to form a vascular network (Fig. 6a). The positive GFP area in the DPSC-bisection
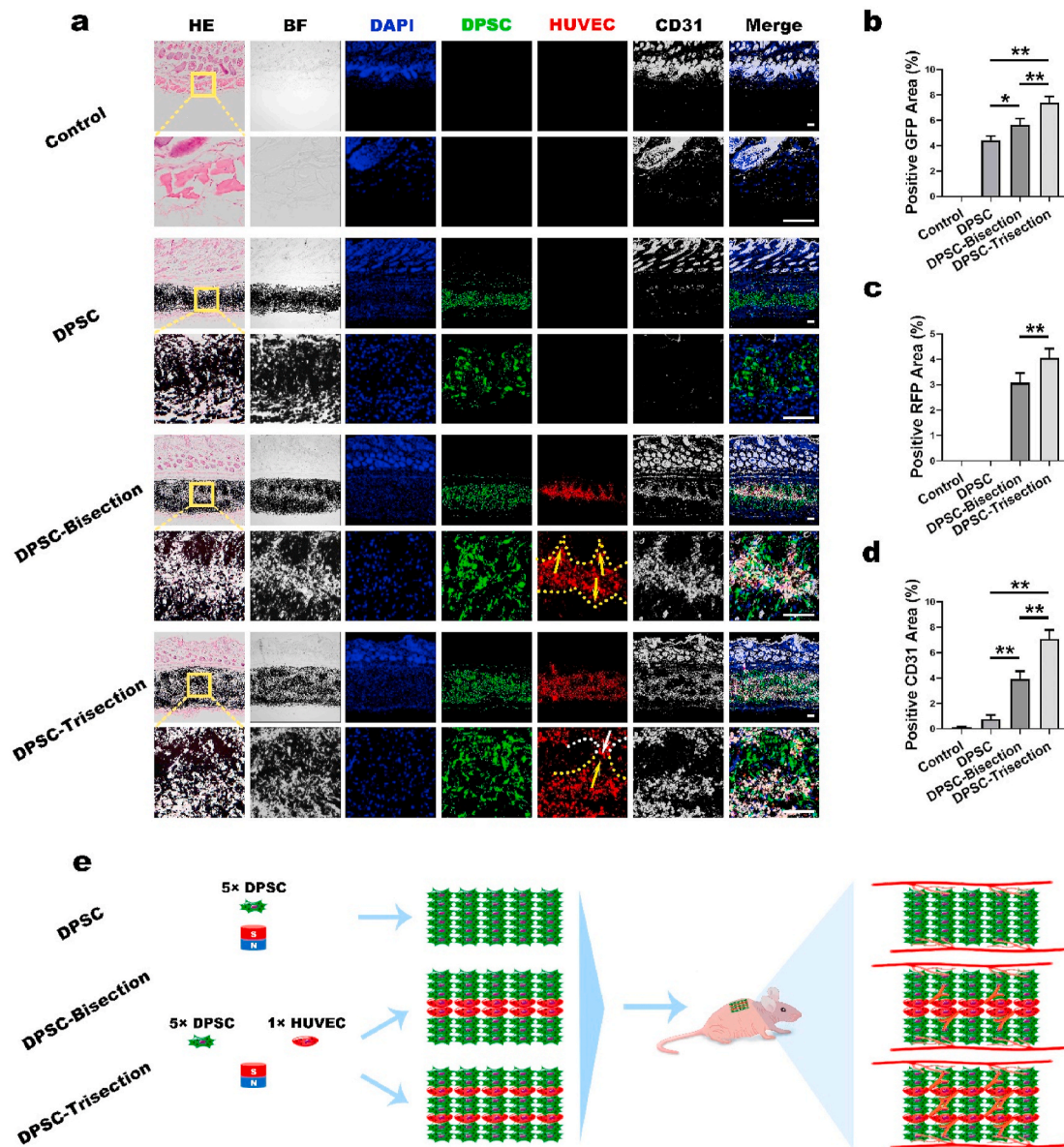
Fig. 6. *In vivo* transplantation of microtissues for 7 days. a) HE staining and CD31 immunofluorescent staining of the Control group, DPSC microtissue group, DPSC-bisection microtissue group, and DPSC-trisection microtissue group (scale bar: 100 μm). The dotted lines in the DPSC-bisection microtissue group show the boundaries of the HUVEC layer. The arrows in the DPSC-bisection microtissue group indicate the HUVEC layer extending to the DPSC layer. The yellow dotted line in the DPSC-trisection microtissue group shows the upper boundary of the lower HUVEC layer. The white dotted line in the DPSC-trisection microtissue group shows the lower boundary of the upper HUVEC layer. The yellow arrow in the DPSC-trisection microtissue group indicates the lower HUVEC layer extending and connecting to the upper HUVEC layer. The white arrow in the DPSC-trisection microtissue group indicates the upper HUVEC layer extending and connecting to the lower HUVEC layer. b) Positive GFP area of four groups. c) Positive RFP area of four groups. d) Positive CD31 area of four groups. e) A schematic diagram of the bisection and trisection architectures of DPSC microtissues to promote vascularization and stem cell survival. The HUVEC layers in the bisection DPSC microtissues can spontaneously extend to the adjacent DPSC layers to promote a rapid vascularization and cell survival. The separated HUVEC layers in the trisection DPSC microtissues can spontaneously extend and connect to each other to form a spatial vascular network to further promote a rapid vascularization and cell survival.

microtissue was higher than that in the DPSC microtissue, while that in the DPSC-trisection microtissue was higher than that in the DPSC-bisection microtissue (Fig. 6b). The positive RFP area in the DPSC-trisection microtissue was higher than that in the DPSC-bisection microtissue (Fig. 6c). The positive CD31 area in the DPSC-bisection microtissue was higher than that in the DPSC microtissue group, and that in the DPSC-trisection microtissue was higher than that in the DPSC-bisection microtissue (Fig. 6d).

These results indicated that the HUVEC layers in the DPSC microtissue improved vascularization and stem cell survival, and the multi-section architecture of the DPSC microtissue was conducive to the extension and connection of separated HUVEC layers. The formation of a

vascular network by the separated HUVEC layers would anastomose with the host vasculature, promoting vascularization and stem cell survival of the DPSC microtissue (Fig. 6e).

The early survival of transplanted stem cell microtissues *in vivo* is a prerequisite for achieving stem cell functions. When the microtissue diameter exceeds 200 μm, rapid vascularization is essential for cell survival by providing oxygen and nutrients and removing waste [28]. In addition, vascularization of microtissues depends on the blood supply at the transplant site. In teeth, the root canal system is narrow and curved, and the narrow apical foramen is the main channel of blood vessels, making vascularization particularly challenging for DPSC microtissue transplantation [31]. In this study, we successfully constructed thick

DPSC microtissues with a diameter of 3.5 mm and a height of 400 μm far exceeding 200 μm. In the DPSC-trisection microtissue, the separated HUVEC layers formed a vascular network and rapidly anastomosed with the host vasculature, which greatly improved the survival of DPSCs. Excellent vascularization and cell survival of DPSC microtissues would provide a crucial basis for future dental pulp regeneration [31]. The rapid magnetic assembly of microtissues with complex architectures *in vitro*, and the rapid vascularization and improved cell survival achieved by the multisection architecture of microtissues *in vivo*, will provide new strategies for stem cell-based therapies, such as vascularized tissue and organ regeneration, and vascularized organoids.

4. Conclusions

The MNP-based magnetic manipulation can rapidly construct stem cell microtissues with complex hierarchical architectures. The cells were magnetically labeled for 1 h, followed by magnetic assembly layer by layer at 5 min intervals, and 24 h later, the microtissues could be transplanted *in vivo*. With the help of the "hamburger" architecture, a spatial network of functional blood vessels that anastomosed with the host vasculature was formed by the separated HUVEC layers as early as 3 days, and stem cell survival was promoted by the rapid vascularization *in vivo*. It is expected that this study will contribute to the future construction and application of structural and functional tissues or organs.

CRediT authorship contribution statement

Yuezhi Lu: Conceptualization, Methodology, Investigation, Writing – original draft. **Chun-Hua Yu:** Methodology, Resources, Writing – review & editing. **Guangzheng Yang:** Investigation, Formal analysis. **Ningjia Sun:** Investigation, Validation. **Fei Jiang:** Methodology, Visualization. **Mingliang Zhou:** Validation, Formal analysis. **Xiaolin Wu:** Software. **Jiaxin Luo:** Data curation. **Cui Huang:** Resources. **Wenjie Zhang:** Conceptualization, Writing – review & editing, Supervision. **Xinquan Jiang:** Writing – review & editing, Project administration, Funding acquisition.

Declaration of competing interest

The authors declare no conflict of interest.

Acknowledgements

Appendix A. Supplementary data

Supplementary data to this article can be found online at https://doi.org/10.1016/j.bioactmat.2021.03.007.

References

[1] C. Loebel, J.A. Burdick, Engineering stem and stromal cell therapies for musculoskeletal tissue repair, Cell Stem Cell 22 (3) (2018) 325–339.

[2] M. De Luca, A. Aiuti, G. Cossu, M. Parmar, G. Pellegrini, P.G. Robey, Advances in stem cell research and therapeutic development, Nat. Cell Biol. 21 (7) (2019) 801–811.

[3] B.D. Sui, C.H. Hu, A.Q. Liu, C.X. Zheng, K. Xuan, Y. Jin, Stem cell-based bone regeneration in diseased microenvironments: challenges and solutions, Biomaterials 196 (2019) 18–30.

[4] J.S. Hyun, M.C. Tran, V.W. Wong, M.T. Chung, D.D. Lo, D.T. Montoro, D.C. Wan, M.T. Longaker, Enhancing stem cell survival in vivo for tissue repair, Biotechnol. Adv. 31 (5) (2013) 736–743.

[5] E.C. Novosel, C. Kleinhans, P.J. Kluger, Vascularization is the key challenge in tissue engineering, Adv. Drug Deliv. Rev. 63 (4–5) (2011) 300–311.

[6] G. Rossi, A. Manfrin, M.P. Lutolf, Progress and potential in organoid research, Nat. Rev. Genet. 19 (11) (2018) 671–687.

[7] S. Grebenyuk, A. Ranga, Engineering organoid vascularization, Front Bioeng Biotechnol 7 (2019) 39.

[8] V.M. Gaspar, P. Lavrador, J. Borges, M.B. Oliveira, J.F. Mano, Advanced bottom-up engineering of living architectures, Adv. Mater. 32 (6) (2020) 1903975.

[9] L. Ouyang, J.P.K. Armstrong, M. Salmeron-Sanchez, M.M. Stevens, Assembling living building blocks to engineer complex tissues, Adv. Funct. Mater. 30 (26) (2020) 1909009.

[10] N. Yamada, T. Okano, H. Sakai, F. Karikusa, Y. Sawasaki, Y.J.M.R.C. Sakurai, Thermo-responsive polymeric surfaces; control of attachment and detachment of cultured cells, Macromol. Rapid Commun. 11 (11) (1990) 571–576.

[11] J. Kobayashi, A. Kikuchi, T. Aoyagi, T. Okano, Cell sheet tissue engineering: cell sheet preparation, harvesting/manipulation, and transplantation, J. Biomed. Mater. Res. 107 (5) (2019) 955–967.

[12] V. Bunpetch, Z.Y. Zhang, X. Zhang, S. Han, P. Zongyou, H. Wu, O. Hong-Wei, Strategies for MSC expansion and MSC-based microtissue for bone regeneration, Biomaterials 196 (2019) 67–79.

[13] C.S. Ong, X. Zhou, J. Han, C.Y. Huang, A. Nashed, S. Khatri, G. Mattson, T. Fukunishi, H. Zhang, N. Hibino, In vivo therapeutic applications of cell spheroids, Biotechnol. Adv. 36 (2) (2018) 494–505.

[14] S. Masuda, T. Shimizu, Three-dimensional cardiac tissue fabrication based on cell sheet technology, Adv. Drug Deliv. Rev. 96 (2016) 103–109.

[15] J.M. Kelm, M. Fussenegger, Scaffold-free cell delivery for use in regenerative medicine, Adv. Drug Deliv. Rev. 62 (7–8) (2010) 753–764.

[16] E.A. Lee, H. Yim, J. Heo, H. Kim, G. Jung, N.S. Hwang, Application of magnetic nanoparticle for controlled tissue assembly and tissue engineering, Arch Pharm. Res. (Seoul) 37 (1) (2014) 120–128.

[17] K. Wu, D. Su, J. Liu, R. Saha, J.P. Wang, Magnetic nanoparticles in nanomedicine: a review of recent advances, Nanotechnology 30 (50) (2019) 502003.

[18] N. Lee, D. Yoo, D. Ling, M.H. Cho, T. Hyeon, J. Cheon, Iron oxide based nanoparticles for multimodal imaging and magnetoresponsive therapy, Chem. Rev. 115 (19) (2015) 10637–10689.

[19] Y. Pan, X. Du, F. Zhao, B. Xu, Magnetic nanoparticles for the manipulation of proteins and cells, Chem. Soc. Rev. 41 (7) (2012) 2912–2942.

[20] S. Tong, H. Zhu, G. Bao, Magnetic Iron oxide nanoparticles for disease detection and therapy, Mater. Today 31 (2019) 86–99.

[21] A. Ito, M. Hayashida, H. Honda, K. Hata, H. Kagami, T. Ueda, T. Kobayashi, Construction and harvest of multilayered keratinocyte sheets using magnetite nanoparticles and magnetic force, Tissue Eng. 10 (5–6) (2004) 873–880.

[22] C. Monzel, C. Vicario, J. Piehler, M. Coppey, M. Dahan, Magnetic control of cellular processes using biofunctional nanoparticles, Chem. Sci. 8 (11) (2017) 7330–7338.

[23] W. Zhang, G. Yang, X. Wang, L. Jiang, F. Jiang, G. Li, Z. Zhang, X. Jiang, Magnetically controlled growth-factor-immobilized multilayer cell sheets for complex tissue regeneration, Adv. Mater. 29 (43) (2017) 1703795.

[24] A.S. Silva, L.F. Santos, M.C. Mendes, J.F. Mano, Multi-layer pre-vascularized magnetic cell sheets for bone regeneration, Biomaterials 231 (2020) 119664.

[25] Y. Xia, J. Sun, L. Zhao, F. Zhang, X.J. Liang, Y. Guo, M.D. Weir, M.A. Reynolds, N. Gu, H.H.K. Xu, Magnetic field and nano-scaffolds with stem cells to enhance bone regeneration, Biomaterials 183 (2018) 151–170.

[26] Y. Lu, W. Zhang, J. Wang, G. Yang, S. Yin, T. Tang, C. Yu, X. Jiang, Recent advances in cell sheet technology for bone and cartilage regeneration: from preparation to application, Int. J. Oral Sci. 11 (2) (2019) 17.

[27] C. Hu, L. Li, Preconditioning influences mesenchymal stem cell properties in vitro and in vivo, J. Cell Mol. Med. 22 (3) (2018) 1428–1442.

[28] S.V. Koduru, A.N. Leberfinger, D. Pasic, A. Forghani, S. Lince, D.J. Hayes, I. T. Ozbolat, D.J. Ravnic, Cellular based strategies for microvascular engineering, Stem Cell Rev Rep 15 (2) (2019) 218–240.

[29] X. Shi, J. Mao, Y. Liu, Pulp stem cells derived from human permanent and deciduous teeth: biological characteristics and therapeutic applications, Stem Cells Transl Med 9 (4) (2020) 445–464.

[30] B. Sui, C. Chen, X. Kou, B. Li, K. Xuan, S. Shi, Y. Jin, Pulp stem cell-mediated functional pulp regeneration, J. Dent. Res. 98 (1) (2019) 27–35.

[31] C. Rombouts, T. Giraud, C. Jeanneau, I. About, Pulp vascularization during tooth development, regeneration, and therapy, J. Dent. Res. 96 (2) (2017) 137–144.

[32] M.W. Laschke, M.D. Menger, Prevascularization in tissue engineering: current concepts and future directions, Biotechnol. Adv. 34 (2) (2016) 112–121.

[33] S. Bersini, I.K. Yazdi, G. Talò, S.R. Shin, M. Moretti, A. Khademhosseini, Cell-microenvironment interactions and architectures in microvascular systems, Biotechnol. Adv. 34 (6) (2016) 1113–1130.

[34] D. Sharma, D. Ross, G. Wang, W. Jia, S.J. Kirkpatrick, F. Zhao, Upgrading prevascularization in tissue engineering: a review of strategies for promoting highly organized microvascular network formation, Acta Biomater. 95 (2019) 112–130.

[35] C. Piard, A. Jeyaram, Y. Liu, J. Caccamese, S.M. Jay, Y. Chen, J. Fisher, 3D printed HUVECs/MSCs cocultures impact cellular interactions and angiogenesis depending on cell-cell distance, Biomaterials 222 (2019) 119423.

[36] R.E. Unger, E. Dohle, C.J. Kirkpatrick, Improving vascularization of engineered bone through the generation of pro-angiogenic effects in co-culture systems, Adv. Drug Deliv. Rev. 94 (2015) 116–125.

[37] H. Zhang, Y. Zhou, W. Zhang, K. Wang, L. Xu, H. Ma, Y. Deng, Construction of vascularized tissue-engineered bone with a double-cell sheet complex, Acta Biomater. 77 (2018) 212–227.

[38] A.J. Deegan, W.J. Hendrikson, A.J. El Haj, J. Rouwkema, Y. Yang, Regulation of endothelial cell arrangements within hMSC - HUVEC co-cultured aggregates, Biomed. J. 42 (3) (2019) 166–177.

[39] N. Sun, S. Yin, Y. Lu, W. Zhang, X. Jiang, Graphene oxide-coated porous titanium for pulp sealing: an antibacterial and dentino-inductive restorative material, J. Mater. Chem. B 8 (26) (2020) 5606–5619.

[40] S. Lin, G. Yang, F. Jiang, M. Zhou, S. Yin, Y. Tang, T. Tang, Z. Zhang, W. Zhang, X. Jiang, A magnesium-enriched 3D culture system that mimics the bone development microenvironment for vascularized bone regeneration, Adv. Sci. 6 (12) (2019) 1900209.

[41] C.A. Schneider, W.S. Rasband, K.W. Eliceiri, NIH Image to ImageJ: 25 years of image analysis, Nat. Methods 9 (7) (2012) 671–675.

[42] Y. Tang, S. Lin, S. Yin, F. Jiang, M. Zhou, G. Yang, N. Sun, W. Zhang, X. Jiang, In situ gas foaming based on magnesium particle degradation: a novel approach to fabricate injectable macroporous hydrogels, Biomaterials 232 (2020) 119727.

[43] S. Zhou, R. Yang, Q. Zou, K. Zhang, T. Yin, W. Zhao, J.G. Shapter, G. Gao, Q. Fu, Fabrication of tissue-engineered bionic urethra using cell sheet technology and labeling by ultrasmall superparamagnetic Iron oxide for full-thickness urethral reconstruction, Theranostics 7 (9) (2017) 2509–2523.

[44] F. Goodfellow, G.A. Simchick, L.J. Mortensen, S.L. Stice, Q. Zhao, Tracking and quantification of magnetically labeled stem cells using magnetic resonance imaging, Adv. Funct. Mater. 26 (22) (2016) 3899–3915.

[45] G. Yang, Y. Lu, C. Liu, M. Zhou, S. Yin, W. Zhang, X. Jiang, A dynamic functional stem cell microtissue culture system based on magnetic nanoparticles labeled endothelial cells, Applied Materials Today 20 (2020) 100691.

[46] C.M. Madl, S.C. Heilshorn, H.M. Blau, Bioengineering strategies to accelerate stem cell therapeutics, Nature 557 (7705) (2018) 335–342.

[47] M. Hippler, E.D. Lemma, S. Bertels, E. Blasco, C. Barner-Kowollik, M. Wegener, M. Bastmeyer, 3D scaffolds to study basic cell biology, Adv. Mater. 31 (26) (2019), e1808110.

[48] S. Ostrovidov, S. Salehi, M. Costantini, K. Suthiwanich, M. Ebrahimi, R. B. Sadeghian, T. Fujie, X. Shi, S. Cannata, C. Gargioli, A. Tamayol, M.R. Dokmeci, G. Orive, W. Swieszkowski, A. Khademhosseini, 3D bioprinting in skeletal muscle tissue engineering, Small 15 (24) (2019), e1805530.

[49] W. Zhang, A. Zhuang, P. Gu, H. Zhou, X. Fan, A review of the three-dimensional cell culture technique: approaches, advantages and applications, Curr. Stem Cell Res. Ther. 11 (4) (2016) 370–380.

[50] F.R. Passanha, T. Geuens, S. Konig, C.A. van Blitterswijk, V.L. LaPointe, Cell Culture Dimensionality Influences Mesenchymal Stem Cell Fate through Cadherin-2 and Cadherin-11, Biomaterials vol. 254 (2020) 120127.

[51] F. Xing, Z. Xiang, P.M. Rommens, U. Ritz, 3D bioprinting for vascularized tissue-engineered bone fabrication, Materials 13 (10) (2020).